Thermal transport-porosity-microstructural characteristics: unpicking the relationship in ultra-porous α-Al2O3 powder

Jordan Letessier, Aïmen E Gheribi, Jean-Mathieu Vanson, Christelle Duguay, Fabrice Rigollet, Nathalie Ehret, Jerôme Vicente, Jean-Laurent Gardarein

Thermal transport-porosity-microstructural characteristics: unpicking the relationship in ultra-porous α-Al_2O_3 powder

Jordan Letessier[a,b,c], Aïmen E. Gheribi[b], Jean-Mathieu Vanson[c], Christelle Duguay[c], Fabrice Rigollet[a], Nathalie Ehret[a], Jerôme Vicente[a] and Jean-Laurent Gardarein[a]

[a]Aix Marseille Univ, CNRS, IUSTI, Marseille, France
[b]Centre for Research in Computational Thermochemistry (CRCT), Department of Chemical Engineering, Ecole Polytechnique, C.P.6079, Succursale Downtown, Montreal, Quebec, Canada H3C3A7
[c]CEA, DES, IRESNE, DEC, Cadarache F-13108 Saint-Paul-Lez-Durance, France

ARTICLE INFO

Keywords:
thermal conductivity
thermal diffusivity
microstructural parameter
multiscale model
intraparticle porosity
interparticle porosity
grain size
measurement
transient hot plate
thermal quadrupole method
inverse problems
X-ray tomography
scanning electron microscopy
theoretical model
percolation theory

ABSTRACT

This study deals with the effective thermal conductivity of porous and ultra-porous unconnected solid phase media composed of α-alumina in air at low temperature (<500K), and at ambient pressure. A multi-scale model is developed, starting from the quantum scale, to describe the conductivity of the single crystal, passing through a microscopic scale to describe the particles (grain size), a mesoscopic scale to take into account the intraparticle porosity and a macroscopic scale with the interparticle porosity. The model is based on percolation theory to describe the strong decrease in conductivity with porosity in this type of medium. This translates into the breaking of contacts between particles past a certain porosity, the critical porosity p_c. This original approach makes it possible to consider this microstructural factor, which accounts for the thermal contacts between particles. These parameters are theoretically deduced or measured for certain samples using an X-ray micro-tomograph (µCT). Combining all these parameters, our model is able to predict 99.7% of the thermal conductivity decay from the pure crystal to the particle bed. Our model proves to be more consistent than current existing models on the same subject. Its validation range extends over the entire porosity range from 0 to 1.

1. Introduction

The Loss of Coolant Accident (LOCA) is one of the postulated accidents for Pressurized Water Reactors (PWR). In such a case, the nuclear pellets can fragment and relocate in its cladding, leading to a degradation of the thermal properties of the fuel rod (Oberlænder and Wiesenack (2014), Boegli and Deissler (1955)). The material is then similar to a granular media with an unconnected solid phase (such as a bed of powder with several particle sizes or packed bed). To understand the behavior of the whole system, it is fundamental to be able to predict the evolution of the thermal properties of this new material. Moreover, as measurements are more expensive and more difficult to carry out in a nuclear environment, we use model materials to perform our parametric study of powder properties. The wide-ranging morphological and granulometric characteristics of α-alumina make it an adequate non-radioactive model material for investigation (Bricout et al. (2013), Giraud et al. (2020)). Furthermore, the study of this material also has advantages for other types of applications.

In fact, the arising interest in ultra-porous alumina materials (i.e. with a porosity greater than 65%) in fields linked to insulation, catalysts, filters or antennae is mainly due to their interesting thermal and mechanical properties: very low density, very resistant to heat, very insulating and possessing large specific surfaces (several m^2/g). They are therefore used as refractory materials, in the manufacture of furnaces and as insulators (Huang and El-Genk (2001)), as a catalyst support (Van Norman et al. (2015)), or in applications related to filtering. They have also shown their usefulness in new applications such as plane antennae, thanks to their electromagnetic properties (Stepanenko et al. (2015)). Moreover, alumina is a cheap material, which makes it a ceramic of choice for industrial applications. Within these ultra-porous materials, a distinction can be made between materials where the solid phase is connected and those where it is not. In the first category, we find foams (Sciamanna et al. (2015), Shimizu et al. (2013)), sintered ceramic fibres (Sun et al. (2014)) and materials manufactured by combining processes such as "the gel-casting process with the pore-forming agent technique", which are processes normally suitable for manufacturing denser materials with porosities less than 65% (Li et al. (2013)). The thermal conductivity of this type of material is rather well described by EMT (Effective Medium Theory) or Maxwell-Hashin-Shtrikman models (Bruggeman (1935), Hashin and Shtrikman (1962)). At equal porosities, connected solid phase materials can have an effective thermal conductivity that is an order of magnitude higher than that of unconnected solid phase alumina. In this study, we therefore focus on the later type of material in order to develop a thermal conductivity model that differs from the usual models used.

In this study, we focus on the description of heat transfer in unconnected solid phase α-alumina with a model based on percolation theory and using microstructural parameters. The thermal conductivity of porous materials depends on

*Corresponding author
ORCID(s):

numerous microstructural parameters such as size and distribution size of pores, grains and particles. The presence or absence of connections between pores and how contacts between particles are defined are also important details to know. However, knowing all these parameters is sometimes impossible or requires a lot of resources. According to the present approach the thermal conductivity of bed of spherical particle can be predicted as a function of porosity via a functional which consider four key microstructural parameters: (*i*) interparticle porosity (p_{inter}), (*ii*) intraparticle porosity (p_{intra}), (*iii*) critical porosity (p_c) and (*iv*) mean grain size ($\langle d \rangle$). The interparticle porosity can be experimentally determined via X-ray micro-tomograph (µCT) which has been done in this work for some of alumina powder samples. The intraparticle porosity is deduced via the relationship between interparticle porosity and the total powder bed porosity (p_e) given by:

$$(1 - p_e) = (1 - p_{inter})(1 - p_{intra}) \tag{1}$$

Where the total powder bed porosity is given by:

$$p_e = 1 - \rho_e / \rho_{theo} \tag{2}$$

Where ρ_e is the effective density of the powder bed and ρ_{theo} is the theoretical density of the solid ($\rho_{theo} = 3.97$ g.cm^{-3} for alumina). Grain size is deduced from supplier data and grain size measurements. The critical porosity is deduced from the results given by the model and from other studies on the subject, described below.

The effective thermal conductivity of particle beds has been thoroughly studied in the literature. Many of these studies are based on a simplified representation of an elementary mesh of the studied porous system, on which the heat transfer mechanisms are composed in parallel or in series (Hadley (1986), Masamune and Smith (1963), Yagi and Kunii (1957), Zehner and Schlünder (1970)). Some of them are based on the effective medium theory (EMT), making it possible to obtain the average values of the physical characteristics of the medium (Bruggeman (1935), Polamuri and Thamida (2015)). All these models do not consider the real microstructure. This is a problem for describing and understanding the critical behavior of thermal conductivity when porosity increases. The universal value of these models is therefore questionable. Our approach, based on percolation theory to model the critical thermal conductivity behavior as a function of porosity of porous materials with unconnected solid phase, claims to be more universal. Models using percolation theory have already been studied in the literature. For example, McLachlan (1987) proposes the coupling of the (EMT) model of Bruggeman (1935) with the theory of percolation to model the electrical conductivity in binary mixtures. Later, this model was used to describe the thermal conductivity of sintered nickel (Deprez et al. (1989)). Ghanbarian and Daigle (2016)) use this model and develop it to model the thermal conductivity in sediments, rocks and soil as a function of water saturation. In Gheribi et al. (2014) and Gheribi et al. (2015) the authors also use the percolation theory to model the thermal conductivity in sintered metals. The critical behavior of the thermal conductivity as a function of porosity is described and interpreted as a second order transition of the continuous phase of the metal. We use this thermodynamic interpretation to establish a model for the thermal conductivity of alumina powders in air. In the present study, the measurements (made on our powders as well as on other ones in literature) cover a wide range of values of mean particle diameters (from 11 nm to 0.4 mm) and the porosity values are quite high (from 42% to 83%), providing different scales of pore sizes in the samples. Our measurements were carried out by a bench using the unsteady hot plane method. The heat transfer mechanisms considered in our study are limited to conduction in the solid phase and in the gas phase. Heat transfer by radiation is neglected because the study temperatures are low (<500 K). Convection will also be neglected, as the pore size of the studied samples is small enough to guarantee a Grashof number below 1000. We are restricting ourselves to the study of the alumina pore system in air.

2. Experimental methods: Thermal conductivity measurement

Thermophysical properties have been measured in our laboratory using a “home-made” experimental setup based on the hot plane method (figure 1) (Maillet et al. (2013), Lahoori et al. (2020)). This experimental bench has been used previously at our laboratory to characterize the thermal properties of different grades of concrete whose composition included different proportions of recycled materials (Sosoi et al. (2022)). A heat flux is imposed on the front face sample during approximately 2 min and the temperatures are measured at both sides. The hot plane is powered by a DC generator, with a power of about 14 W. The temperature measured at the front face is imposed as the Dirichlet condition in the thermal model. This calculation gives the temperature on the rear face. It is then compared with the measured rear face temperature and the thermal parameters are estimated by minimizing the difference between these two signals. The use of the measured front face temperature as the Dirichlet condition eliminates the need to know exactly the time shape and the exact value of the flux delivered by the power supply. It is this temperature evolution recorded at the front face ($\theta_{meas}(0, t)$) that serves as the input excitation for the model (8), it is called "the transmittance-based model" (Maillet et al. (2013), Lahoori et al. (2020)). The use of thermal grease between the thermocouples and the base plates limits the thermal contact resistance. A fibrous insulator is placed around the device to promote 1D transfer between the two faces. The 3 thermograms measured on the front and rear faces allow us to ensure the uniformity of the temperature on each face (figure 2). Once this verification is established, the thermogram measured by the central thermocouple is injected into the model. The standard deviation of the measurement noise is approximately 0.01°C for a heating of 2°C on the rear face and 7°C on the front face. We model the

powder bed as a homogeneous medium in perfect contact with a semi-infinite medium on the rear face. Using the thermal quadrupole formalism (Maillet et al. (2000)) to relate, in Laplace space, the heating and fluxes between the front face ($\bar{\theta}(0, p_{Lp})$, $\bar{\phi}(0, p_{Lp})$) and the rear face ($\bar{\theta}(e + e_s, p_{Lp})$, $\bar{\phi}(e + e_s, p_{Lp})$), the thermal model equation can be written as:

$$\begin{pmatrix} \bar{\theta}(0, p_{Lp}) \\ \bar{\phi}(0, p_{Lp}) \end{pmatrix} = C\,B \begin{pmatrix} \bar{\theta}(e + e_s, p_{Lp}) \\ \bar{\phi}(e + e_s, p_{Lp}) \end{pmatrix} \tag{3}$$

$$\text{With, } B = \begin{pmatrix} 1 & 0 \\ x_4\ p_{Lp} & 1 \end{pmatrix} \text{ and,} \tag{4}$$

$$C = \begin{pmatrix} \cosh\left(\sqrt{x_1\ p_{Lp}}\right) & \frac{1}{x_2\ \sqrt{p_{Lp}}} \sinh\left(\sqrt{x_1\ p_{Lp}}\right) \\ x_2\ \sqrt{p_{Lp}}\ \sinh\left(\sqrt{x_1\ p_{Lp}}\right) & \cosh\left(\sqrt{x_1\ p_{Lp}}\right) \end{pmatrix} \tag{5}$$

$x_1 = e^2/\alpha$ and, $x_2 = b$ with, p_{Lp} the Laplace variable (s^{-1})

The matrix B represents a copper plate of thickness e_s. Its small thickness and high conductivity allow it to be modelled as a purely capacitive layer. Matrix C represents the powder bed as an equivalent homogeneous material of thickness e, diffusivity α and effusivity b. The boundary condition on the PVC block, assumed to be semi-infinite (characteristic diffusion time $t_{diff}^{PVC} \approx 10^4$ s for a measurement time of about 800 s), allows to relate the flux and the rear face heating by:

$$\bar{\phi}(e + e_s, p_{Lp}) = \quad x_3\ \sqrt{p_{Lp}}\ \bar{\theta}(e + e_s, p_{Lp}) \tag{6}$$

By expanding equation (3) and applying it for a unit Laplace heating on the front face $\bar{\theta}(0, p_{Lp}) = 1$, the resulting Laplace heating on the back face corresponds to the transmittance of the system $\bar{\theta}_{imp}(e + e_s, p_{Lp})$:

$$\bar{\theta}_{imp}(e + e_s, p_{Lp}) = \left[\cosh\left(\sqrt{x_1\ p_{Lp}}\right) + \left(\frac{x_4}{x_2}\sqrt{p_{Lp}} + \frac{x_3}{x_2}\right) \sinh\left(\sqrt{x_1\ p_{Lp}}\right)\right]^{-1} \tag{7}$$

The inverse Laplace transform (performed with De Hoogs algorithm (De Hoog et al. (1982))) of the system transmittance ($\bar{\theta}_{imp}(e + es, p_{Lp})$) then provides the impulse response of the modelled system.

$$\theta_{mod}(e + e_s, t) = \quad \mathcal{L}^{-1}\{\bar{\theta}_{imp}(e + e_s, p_{Lp})\} \circledast \theta_{meas}(0, t) \tag{8}$$

The modelled rear face heating versus time $\theta_{mod}(e + e_s, t)$, is then calculated by time convolution (denoted $\circledast$) between this impulse response and the measured front face thermogram (eq: (8)). In equation (7), it can be seen that the model transmittance of the system depends on only 4 parameters: x_1 [s] and x_2 [$Jm^{-2}K^{-1}s^{-1/2}$] are the apparent diffusion time and the equivalent effusivity of the particle bed respectively, x_3 [$Jm^{-2}K^{-1}s^{-1/2}$] is the effusivity of the PVC block and x_4 [$JK^{-1}m^{-2}$] is the surface capacitance of a copper sole. The orders of magnitude for the values of these parameters are: $x_1 \approx 500$ s, $x_2 \approx 400$ $Jm^{-2}K^{-1}s^{-1/2}$, $x_3 \approx 518$ $Jm^{-2}K^{-1}s^{-1/2}$ and $x_4 \approx 3400$ J $K^{-1}m^{-2}$.

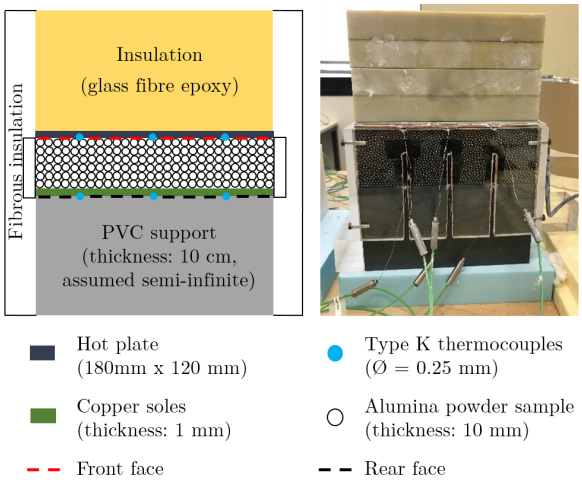

Figure 1: Schematic and photo of the experimental diffusivity measurement bench (photo taken without fibrous insulation)

A sensitivity study shows that the surface capacitance of the soles x_4 is a low-sensitivity parameter of the model, so it will be fixed at its nominal value. In addition, the effusivity of the rear PVC sample holder has been measured by our device (with other sample holders) and by two subcontractors on the other hand, so it will also be fixed. Only the two parameters x_1 and x_2 remain to be estimated. Solving the problem by the inverse method involves adjusting x_1 and x_2 to minimize the RSS (Residual Sum of Squares) that measures the discrepancy between the measured $\theta_{meas}(e + e_s, t)$ and modelled $\theta_{mod}(e + e_s, t)$ rear face heating. To solve this Ordinary Least Squares problem, we use the Gauss-Newton algorithm. The figure 2 shows the measured thermograms (front face and rear face) as well as the optimal modelled thermogram on rear face, computed with the identified parameters. The residuals between measured and modelled thermograms are also shown and their statistics (mean and standard deviation) are close to those of measurement noise, which gives confidence to the model. In addition, some of the measurements were verified with other experimental setups (Transient Hot Bridge by Linseis and hot disc method, both methods are suitable for measurements on powders (Lager et al. (2019), (Predeep and Saxena (1997)). The values of x_1 and x_2 obtained after minimization give us α and b and we can deduce the equivalent bed conductivity $\lambda = x_2\sqrt{e^2/x_1} = b\sqrt{\alpha}$. For each estimated parameter, an uncertainty is calculated, corresponding to the sum of errors due to measurement noise and to the propagation of uncertainties of the fixed parameters assumed to be known (Rigollet and Le Niliot (2011), Aster et al. (2018)), which is estimated to be 10%. It can be seen that the overall

uncertainty for a parameter corresponds essentially to the propagation of the uncertainties of the fixed parameters.

3. Theoretical description of the thermal transports within ultra-porous materials

The thermal conductivity of powder beds depends on thermodynamic parameters such as temperature, and microstructure-related parameters such as the size, size distribution of pores and grains and particles. The presence of phase compositions due to impurities or mixtures of chemical compounds can also significantly affect the effective thermal conductivity value of powder beds. These parameters variations can lead to an order of magnitude variation in the thermal conductivity of the same dense material. Measuring each microstructural parameter and knowing the variations of the conductivity as a function of these parameters is very complex. We assume that the powders studied consist of porous particles composed of grains (figure 3). We have therefore defined a limited set of parameters which are, according to the literature, the most impactful (Yagi and Kunii (1957), Francl and Kingery (1954), Gheribi and Chartrand (2015)). Firstly, we have chosen to distinguish intraparticle p_{intra} from interparticle p_{inter} porosity. Most studies do not make this distinction and thus omit an important feature of the microstructure of the media, especially in the case of ultra-porous powders where high porosity cannot be explained without considering these two scales of porosity. Our model is a multi-scale description of the effective thermal conductivity of a powder bed. Starting from the thermal conductivities of the microscopic elements that make up a powder bed, we can trace the thermal conductivity of the whole at a macroscopic scale. The conductivity can be described as follows:

$$\lambda_e^{mod}(T,\langle d\rangle,p_{intra},p_{inter},p_c,n_c) = \underbrace{\lambda_{sc}(T)M(T,\langle d\rangle,p_{intra})}_{\lambda_p}\underbrace{N(p_{inter},p_c,n_c)}_{\substack{\text{macrostructural}\\ \text{factor}}} + \underbrace{p_e\lambda_{air}(T)}_{\substack{\text{contribution}\\ \text{of air}}} \quad (9)$$

The conductivity of the medium is considered as a parallel model, the first term corresponds to heat transfer in the solid phase (considering the contacts between particles) and the second term to heat transfer in the gas phase. The function M reflects the reduction of the thermal conductivity of a particle λ_p with respect to that of the single crystal λ_{sc}, as a function of temperature T, the average grain size $\langle d\rangle$ and the intraparticle porosity p_{intra}. Usually, ceramics have a polycrystalline solid phase and therefore their conductivity is different from that of the single crystal (λ_{sc}). The difference between the conductivity of a polycrystal and that of a single crystal depends directly on its grain size. The smaller the grain size is, the greater the specific amount of grain boundaries is, which increases the thermal resistance and degrades the thermal conductivity. Thus, the conductivity of the solid phase of a dense powder particle λ_g can be described as in equation (10).

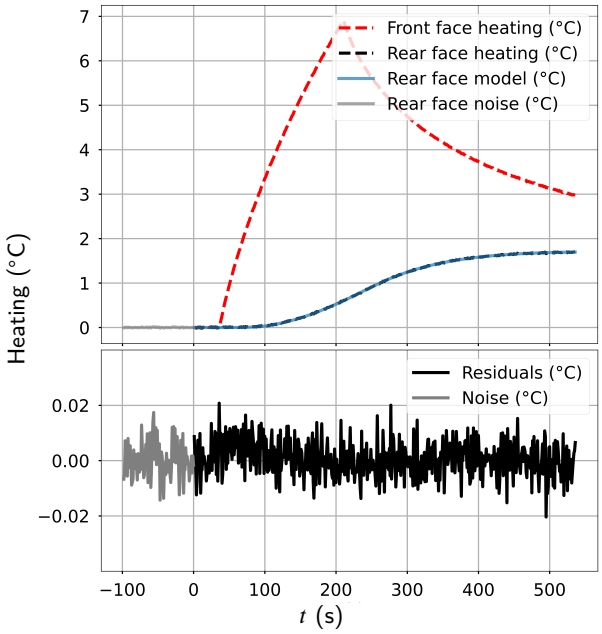

Figure 2: Top : typical thermograms provided by the Hot Plane set-up and its modelization : front face and rear face measured heatings (respectively red and black dashed lines), rear face model (blue line), rear face noise (grey line). Bottom : rear face noise (grey) and residuals (black).

$$\lambda_g(T,\langle d\rangle) = \lambda_{sc}(T)\underbrace{\left[1-u\arctan\left(1/u\right)\right]}_{g(T,\langle d\rangle)} \quad (10)$$

Where g is a function that considers this degradation as a function of the average grain size ($\langle d\rangle$, eq:(10), Gheribi and Chartrand (2015)). $u^2 = \sigma(T)/\langle d\rangle$, where σ is a characteristic length of the material which represents the reduction of the mean free path of phonons, due to grain boundaries. λ_{sc} represents the thermal conductivity of the pure crystal ($W.(mK)^{-1}$). Its expression as a function of temperature (eq: (11) valid from room temperature to melting point) has been determined in a purely theoretical manner (Gheribi and Chartrand (2012), Julian (1965)). It can be written as:

$$\lambda_{sc}(T) = A.\frac{\bar{M}\theta_D^3\delta(T)}{\gamma^2 T n^{2/3}} \quad (11)$$

where $\bar{M}$ is the average atomic mass (in amu), δ^3 is the volume per atom (δ in Å), θ_D is the Debye temperature in K, n is the number of atoms per primitive cell and the constant $A = (2.43\times10^{-8})/(1-0.514/\gamma+0.228/\gamma^2)$.

The thermal conductivity of a dense particle is therefore at most equal to $\lambda_g = \lambda_{sc}\ g(d_p)$, with d_p being the diameter of the particle. Depending on the manufacturing process, the powder particles can be dense or porous. For example, in the case of aggregates, the particles have an internal porosity which we call p_{intra}. Assuming that intraparticle porosity

is homogeneously distributed, we describe the conductivity λ_p of a porous particle as in equation (12). This difference between intraparticle and interparticle porosity (p_{inter}) allows us to consider one aspect of the microstructure of the particules themselves, beyond the macroscopic porosity associated to their arrangement into the powder.

$$\lambda_p(T, \langle d \rangle, p_{intra}) = \lambda_{sc}(T) \underbrace{g(T, \langle d \rangle)\,(1 - p_{intra})}_{M(T, \langle d \rangle, p_{intra})} \tag{12}$$

$$\lambda_e^{mod}(T, \langle d \rangle, p_c, n_c, p_{inter}, p_{intra}, p_e) = \lambda_p(T, \langle d \rangle, p_{intra}) \times \underbrace{(1 - p_{inter})\, f_c(p_c, p_{inter}, n_c)}_{N(p_{inter}, p_c, n_c)} + p_e \lambda_{air}(T) \tag{13}$$

By multiplying equation (12) by $(1 - p_{inter})$, we obtain the maximum thermal conductivity of the solid phase of the medium. However, the conductivity of an unconnected solid phase porous medium is often far from this value. This is due to a second order transition of the conductivity with the porosity. This effect is expressed by the factor $f_c(p_c, p_{inter}, n_c)$, corresponding to the critical function that will be detailed later. More over, in order to take into account the heat transfer in air, we consider it as a parallel mechanism to the transfer in the solid phase. The latter is equal to the effective porosity of the bed p_e, multiplied by the conductivity of air λ_{air}. The expression of λ_{air} as a function of T is given by a third order polynomial fitted to the measurements of Lemmon and Jacobsen (2004).

The thermal conductivity of an unconnected solid phase porous medium λ_e^{mod}, is then written as in equation (13). Figure 3 gives an order of magnitude of the conductivity values according to the different scales of observation. The f_c function is a critical function inspired by the one used by Inden (1976) for second order ferromagnetic transitions. In our case, it gives information on the connection between the particles and translates the critical behavior of the diffusivity of the solid phase (α_s) as a function of porosity. f_c is defined as follows:

$$f_c(p_c, p_{inter}, n_c) = 1 + \int_0^{p_{inter}} \chi(p_c, p, n_c)\, dp \tag{14}$$

$$\chi(\tau, n_c) = \begin{cases} A \ln\left(\frac{1+\tau^3}{1-\tau^3}\right), & 0 \le p < p_c \\ A\left(\ln\left(\frac{1+\tau^{-n_c}}{1-\tau^{-n_c}}\right) - \ln\left(\frac{1+p_c^{n_c}}{1-p_c^{n_c}}\right)\right), & p_c < p \le 1 \end{cases} \tag{15}$$

Note that $\tau = p/p_c$. The function χ corresponds to the derivative of the diffusivity of the solid phase α_s with respect to the porosity p, $\chi = \partial\alpha_s/\partial p$, it is normalized and its integral on $[0, 1]$ is equal to -1. The boundary conditions are written in such a way that χ is defined on a bounded and closed interval ($p \in [0, 1]$, $\chi(p = 0) = 0$ and $\chi(p = 1) = 0$, A = -1). Parameters p_c and n_c

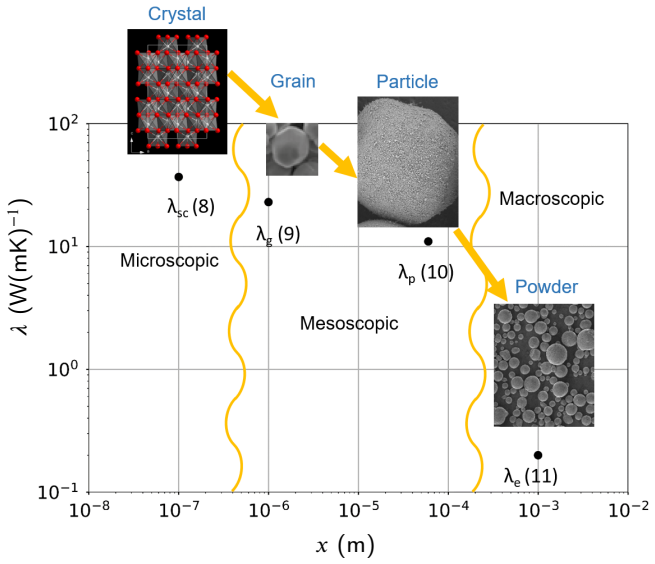

Figure 3: Thermal conductivity of α-alumina powder as a function of the scale of study. The thermal conductivity values are the typical values issued from our measurements.

correspond to the percolation threshold (critical porosity) and to a critical exponent of the function, which depends on the material used (we describe thereafter how we fixed it for α-alumina). The critical exponent for the first part of the χ function is fixed at 3, corresponding to a thermodynamic phase transition (Inden (1976)). The percolation threshold (identified as critical porosity in the present study) depends on the composition of the filling gas (Air, He, N_2, Ar) and its pressure and several microstructural parameters related with both porosity and particle: pore shape, pore size, pore distribution, inclusion shape, particle shape. In the present work, it is intended to describe the percolation effect upon the thermal transport from an effective point of view i.e the critical porosity is not only defined through the definition of the percolation threshold of a given geometrical configuration considering the particles coordinations (1^{st} nearest neighbor and beyond). If the interparticle porosity is lower than p_c, the effective thermal connections between the particles are numerous. If it is higher, the number of effective thermal contacts decreases sharply, the particles are no longer thermally connected to each other. The thermal resistance across particle-particle boundaries is the major factor in the dumping of the geometrical porosity threshold. Several experimental studies on the thermal transport within spherical particle-based sintered metal show a drastic decrease in thermal conductivity (diffusivity) around a porosity level lying between 0.11 and 0.24, with an average value of 0.16 and a relatively small standard deviation (Gheribi et al. (2014), Gheribi et al. (2015)). For instance, the critical porosity of AISI 316L stainless steel is 0.11, that of sintered copper is 0.16, and about 0.24 for sintered tungsten samples. These values are very close to site percolation thresholds of 3D systems. For site percolation in a 3D system with a coordination number of 8, $p_c = 0.245$ (Van Der Marck

(1998)). By varying the coordination number to 14, i.e. taking second neighbors into account, the site percolation threshold decreases to 0.168 (Jerauld et al. (1984)). An accurate value for the effective thermal coordination number is therefore one of the important parameters to know in order to best estimate the effective thermal conductivity of a powder bed.

Identification of the critical exponent

The value of the critical exponent n_c in equation (15) is linked to the slope of f_c in the neighborhood of p_c. The larger this exponent is, the faster χ tends towards infinity, and therefore the steeper is the decrease in f_c. It reflects the behavior of the thermal conductivity at the transition from the connected state of the particles to an unconnected state. The value of n_c is specific to the used material, in our case α-alumina. We can therefore, thanks to the various data in the literature listed in this paper, determine its value. To do this, we fixed all the parameters of the model presented in equation (13) with the values given in table 1. We have fixed the parameter p_c to 0.168. p_{inter} varies between 0.33 and 0.42 when its value is not known. This range was chosen considering that the porosity of a bed of randomly arranged dense particles lies in this range (Dullien (2012), Van Norman et al. (2015)). The value of 0.168 corresponds, as explained above, to the site percolation threshold of a cubic system centered on 14 neighbors. We calculate the optimal value of n_c to minimize the squared deviation between the measurement points and the model for each study, and then we take the average value of all the studies. The results are shown in figure 4a. We find that the average value of n_c lies between 4.48 and 5.56. We can see that the results are close for the different studies, except for Laubitz (1959) and Van Norman et al. (2015), having n_c values closer to 3. This difference may be due to different factors. For example, the arrangement may be different and the fact that p_c is fixed adds an uncertainty that is not considered in the vertical estimation bars. The interparticle porosity values mentioned by the authors may also be different from reality when measuring conductivities. By doing the opposite, i.e. by imposing the critical exponent n_c at 5.02, we looked at the optimal values of p_c for each study (figure 4b). The variations are slight and centered around 0.17. In Laubitz (1959) and Van Norman et al. (2015), p_c rather seems to be around 0.25. This value corresponds to a cubic arrangement with a coordination number of 8, which is quite feasible. The small variation of these parameters shows the consistency of our statement that n_c is fixed and depends only on the material properties, and that the uncertainties on its determination come from the uncertainties on the coordination of the studied powders. In any case, the observed values of critical exponents correspond to typical values of thermodynamic phase transitions (Inden (1976)).

4. Results and discussion

Our data

Our study started with thermal conductivity measurements in ultra-pure (>99.9%) α-alumina powders. These samples were chosen for their different microstructural properties, dependent on the manufacturing processes used. A first family of powders is derived from the spray dried process and a second one from the Bayer process (BP). For each family, we studied several samples of powders with average particle sizes ranging from about 1 µm to about 70 µm. The powder data is presented in table 1. The first column corresponds to the average value of the grain size ($\langle d \rangle$) making up the particles. From the specifications given by the suppliers and the analysis of the SEM images, we can approximate the grain size around 0.1 µm and 5 µm, for the alumina powders of our study. For measurements where $\langle d \rangle$ is not given, it is assumed that the grain size is equal to the particle size (d_p). This corresponds to the maximum conductivity, that of a single crystal of size d_p. For our samples, the mass and volume measurements introduced into the experimental device give us the effective density of the sample ρ_e. And allows us to determine p_e (see equation (2)).

The granulometry was measured by laser diffraction (wet dispersion method), with at least 2 measurements per powder. The values presented in table 1 were obtained without the application of ultrasound. Measuring the interparticle porosity of powders is complicated, because the particle size is small and the pore size in the particles is too large to be measured by the BJH method (the pores of the particles are larger than 50 nm). This method consists of determining the pore size distribution of a medium by studying the variations between the adsorption and desorption of a gas in the medium. We therefore measured p_{inter}, for two samples, using an X-ray micro-tomograph (µCT) EasyTom XL 150-160 from Rx-Solution, with a HAMAMATSU microfocus X-Ray source Modèle L 10711-23 (current= 47 A, voltage = 127 V, voxel size 1.5 µm). Due to the constraints of the µCT measurement, the sample holder is different from the one used for the conductivity measurement. This creates an uncertainty on the announced interparticle porosity values because it is not measured directly on the same part of the sample than the conductivity measurements. However, total porosity measurements were carried out in different containers. These measurements showed a small variation in the overall porosity, indicating that the arrangement of the particles does not vary much depending on the container. The container is considered as a representative volume of the medium. The measurement and processing of the images obtained with the tomograph give an uncertainty on p_{inter} of about 1 % due to segmentation. Recall that p_{inter} corresponds to the interparticle or inter-aggregate porosity (in the case where the powders are composed of aggregates, i.e. porous particles with $p_{intra} \neq 0$). p_{inter} is measured for samples 5 and 6 from the spray dried process. Both samples have a similar particle size, with a monomodal distribution

Table 1
Properties and parameters of the powder bed samples used in different studies (our measurements made by X-ray tomography are marked by *)

Studies	$\langle d \rangle$ (µm)	d_p (µm)	p_e	p_{inter}	T_{meas} (K)	λ_e^{meas} (W(mK)$^{-1}$)	n °
This study							
spray-dried α-alumina (SD)		1.35	0.83		298	0.089	1
		4.93	0.645		298	0.083	2
	0.1	23.3	0.66		298	0.122	3
	0.1	44.8	0.66		298	0.127	4
	0.1	56.4	0.70	0.405 ± 0.005*	298	0.106	5
	0.1	65.8	0.66	0.37 ± 0.004*	298	0.202	6
This study							
α-alumina produced by Bayer process (BP)		1.63	0.72		298	0.092	7
		7.23	0.71		298	0.109	8
	5	49	0.73		298	0.178	9
	5	82.25	0.73		298	0.179	10
Laubitz (1959)		80	0.75		473	0.22	11
		400 ± 100	0.525	0.505	473	0.376	12
Luikov et al. (1968)		60	0.75		300	0.171	13
		263	0.42		373	0.42	14
Shapiro et al. (2004)		60	0.46		333	0.21	15
		166	0.51		333	0.286	16
		211	0.42		333	0.381	17
Hu et al. (2007)		0.011	~ 0.8		300	0.035	18
		0.3	~ 0.8		300	0.085	19
		0.5	~ 0.8		300	0.105	20
Van Norman et al. (2015)		90	0.83	$0.33 - 0.37$	320	0.48	21
Pujula et al. (2016)		125	0.745		293	0.11	22

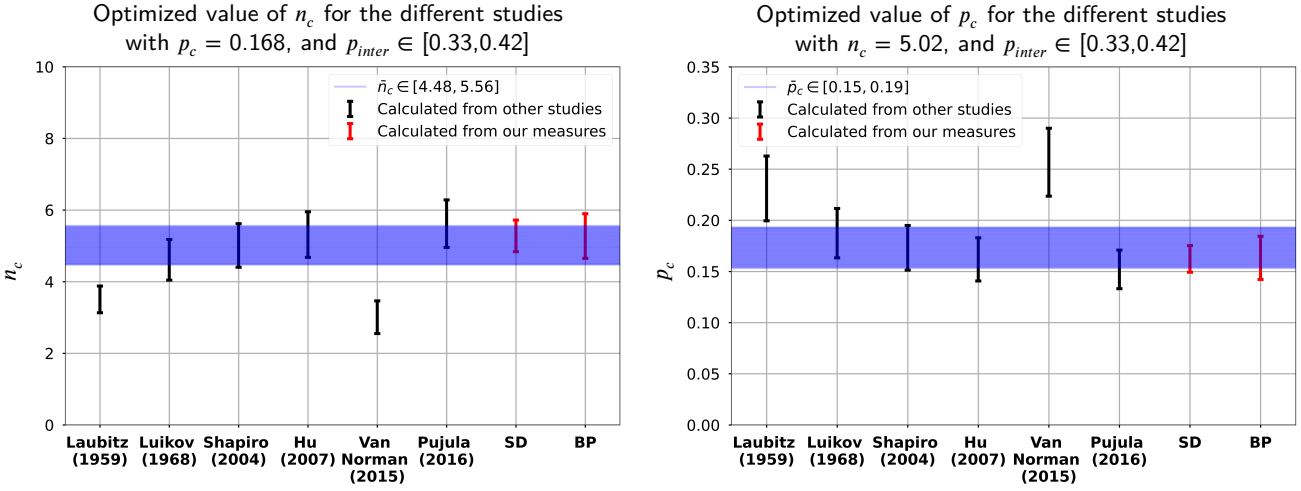

(a) (b)

Figure 4: (**a**) Plot of the critical exponent n_c for different studies with p_c fixed at 0.168 and p_{inter} varying from 0.33 to 0.42 except for values where p_{inter} is known (see table 1). (**b**) Plot of the critical porosity p_c for different studies with n_c fixed at 5.02 and p_{inter} varying from 0.33 to 0.42 except for values where p_{inter} is known (see table 1)

centered at about 60 µm. However, sample 5 is composed of spherical particles with homogeneous porosity and sample 6 of particles with pores of several micrometers in their centre. Their appearance is hollow. Both aspects were observed by µCT and scanning electron microscopy (SEM, see figure 5). Figure 5.a corresponds to sample 6 and figure 5.b to sample 5. The pictures on the left correspond to a slice of the µCT measurement stack for the two samples, the images in the centre were obtained after segmentation and after filtering of the original images by a median filter 3 voxels in width. Then, the picture on the right shows SEM images of the corresponding powders. For the µCT slice of powder

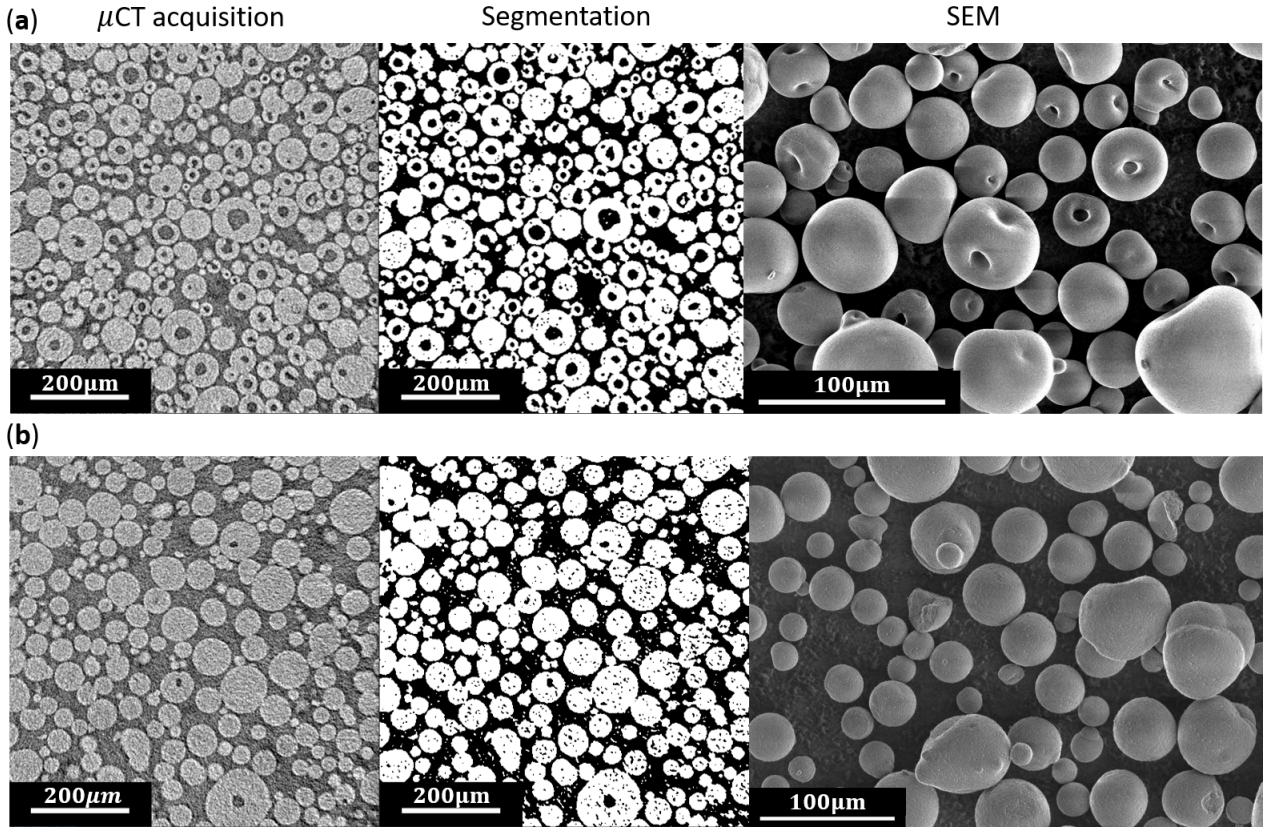

Figure 5: Original μCT images of slices, images after segmentation and after applying a median filter and SEM images for two different samples (**a**) corresponds to the n °6 SD sample with d_{50} = 65.8 μm and (**b**) corresponds to the n °5 SD sample with d_{50} = 56.4 μm.

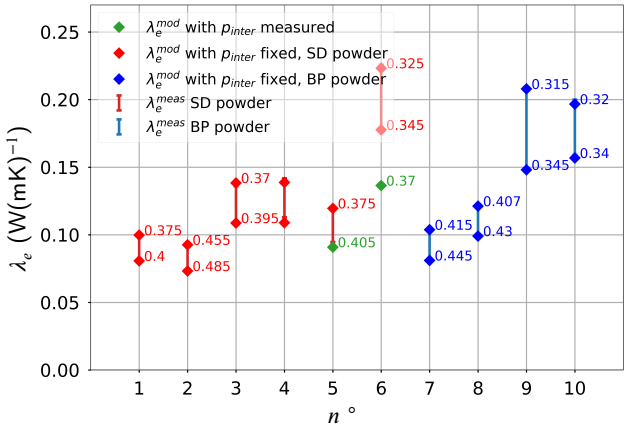

Figure 6: Optimised range of p_{inter} (marked by diamonds) given by our model for our thermal conductivity measurements. The numbering on the x-axis corresponds to the numbering used in the table 1. Labels attached to the the bars show the p_{inter} porosity range for each measurement.

6, we can see the hollows in the centre of the particles. In the SEM images we can see that, for most of the particles of powder 6, the hollow communicates with the outside. These hollows favor the entanglement of the particles with each other, which also favors thermal transfer. The interparticle porosity measured for powders 5 and 6 is 0.405 and 0.37 respectively. Figure 6 shows the measured thermal conductivities for the different SD and BP powders and their error bars. It also shows the range of possible interparticle porosities predicted by the model (red diamonds for SD powders and blue diamonds for BP powders). Interparticle porosity measurements made at the μCT are displayed by green diamonds. The model parameters are n_c = 5.02 and p_c = 0.168. We can observe that the range of p_{inter} values predicted by the model for sample 6 excludes the value measured at the μCT (0.37 $\notin$ [0.325, 0.345]). This difference can be explained by the fact that we assume the critical porosity to be 0.168. However, the μCT and SEM images (figure 5) show that the particles of powder 6 are hollow and open on the outside. This can lead to entanglements and therefore to a smaller effective thermal coordination number and a larger p_c. The measured value would correspond to a p_c = 0.188. Furthermore, the grain size distribution influences this parameter and it can be observed that it is not the same for both samples. In general, we observe that the thermal conductivity predicted by the model is very sensitive to the interparticle porosity. This highlights, once again, the importance of the microstructural parameters p_c and p_{inter}.

Other thermal conductivity data of non connected solid phase alumina

Figure 7 presents the results obtained for the prediction of our model of thermal conductivity of alumina powders for different studies. As before, the critical porosity and critical exponent are fixed and equal to 0.168 and 5.02, respectively. The vertical bars correspond to the range of possible values, to which λ_e^{mod} belongs for p_{inter} between 0.33 and 0.42. We can see that the model is sensitive to this parameter. The average sensitivity of the model for these data is about 0.015 W.(mK)$^{-1}$ per percent of interparticle porosity. Knowledge of the microstructural parameters for predicting the effective conductivity is essential. The horizontal error bars correspond to the uncertainty of the measurement. The closest prediction is for Laubitz (1959) measurement ($n°12$ in table 1). However, this is a point where the interparticle porosity is known. This discrepancy, as mentioned in the previous section, may be due to the fact that p_c was assumed to be constant, whereas it also depends on the microstructure. For the same reason, the measurement of Van Norman et al. (2015) is also above the prediction of our model. Moreover, the measurements of Laubitz (1959) were made at temperatures of 473 K. It is possible that radiative transfer increases the effective thermal conductivity compared to that predicted by our model, which does not consider this mode of transfer. The possible values are given in the range plus or minus 0.1 W(mK)$^{-1}$. An exact knowledge of the microstructure would allow us to be more precise and to have a better estimate of p_c, making the model more consistent.

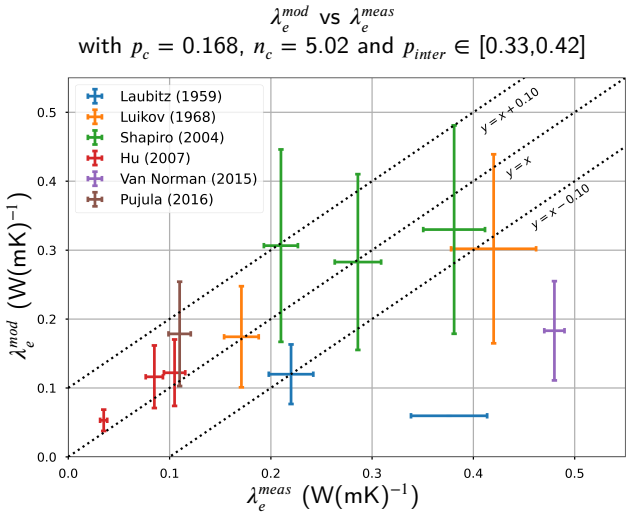

Figure 7: Correlation of experimental and predicted thermal conductivity of α-alumina powder with n_c fixed at 5.02. The horizontal error bar corresponds to the measurement error and the vertical bars represent the values taken by λ_e^{mod} when p_{inter} varies from 0.33 to 0.42

Other models

In this section we compare our model to models often cited in the literature, the expressions of the models are presented in table 2. It is important to distinguish experimental correlations from theoretical models. In the first category, we are interested in the models of Kunii and Smith (1960) and Hsu et al. (1995), two models with localized parameters (the heat transfer is described from an elementary cell representing the elementary mesh of the medium). In Kunii and Smith (1960) the cell is 2D reduced to two spheres in contact and for Hsu et al. (1995) the cell is 3D cubic, with an unidirectional heat flow. The latter gives the most satisfactory results of the three models presented in his paper. A parameter, γ_c, represents the ratio between the contact width between two solid elements and the width of the solid cube, allowing us to have an expression of the model in the case of unconnected solid particles, when γ_c tends towards 0. These models are calibrated by the authors with experimental measurements and have a good agreement with the conductivity of different particle beds. Models from effective media theory are also often cited in this field. We choose to compare our model with the model of Bruggeman (1935). Figure 9 represents the thermal conductivity as a function of porosity p_e given by the different models for α-alumina at 293 K. The models quoted depend on the porosity p_e and the conductivities of the two phases. For our model, we have considered dense particles, i.e. without intraparticle porosity, and with a maximum grain conductivity equal to that of the crystal. This corresponds to the curve given for $p_{intra} = 0$ in figure 8. It can be seen that the predictions of our model fall between the correlation models and the EMT model, when p_e is less than 0.4. The conductivities predicted by Hsu et al. (1995) are not realistic when $p_e < 0.2$. The conductivity decreases sharply with p_e, even for porosities close to 0, this has no physical correlation because, for these porosities, the links between particles are numerous, conduction is mainly through the solid phase and not through the fluid phase. The model of Kunii and Smith (1960) is defined for $0.26 < p_e < 0.476$ and is approximated on the other intervals (this explains the slight discontinuities at the ends of the interval). The approximation proposed by Kunii and Smith (1960) for low porosities can be questioned. Indeed, the conductivity when $p_e = 0$ does not tend towards the value of the conductivity of the solid phase. The conductivity according to Bruggeman (1935) decreases linearly until about $p_e = 0.65$, this approach is also in contradiction with the experiments. For example, assuming that the particles in the powder bed of Shapiro et al. (2004) with $p_e = 0.42$ are dense (i.e. in the case where the thermal conductivity would be the highest), we have $\lambda_e^{meas} = 0.381$ W(mK)$^{-1}$ and the EMT model predicts $\lambda_e^{EMT} = 14.7$ W(mK)$^{-1}$. More than an order of magnitude separates these two values. Of all these models, our model seems to be the most consistent with the data reported in the literature, whatever the considered porosity. It can be noted that our model and the model of Hsu et al. (1995) (unconnected particles) are very close when $p_e > 0.6$. This is in agreement with the theory of our model which predicts a break in the connections between particles as soon as the total porosity exceeds the critical porosity p_c. The models of Hsu et al. (1995) (connected particles) and Kunii and Smith (1960) assume a constant exchange surface between

the particles, whatever the porosity, over the interval [0, 1] and [0.476, 1]. These models are not suitable for modelling the conductivity of ultra-porous powders, where this area decreases with increasing porosity.

Figure 8 is a 2D map of the values predicted by our model for alumina at T=293K, $\langle d \rangle$=∞, p_c=0.168 and n_c=5.02 as a function of p_{inter} and p_{intra}. The grey lines are thermal iso-conductivity and the pink to yellow lines are total iso-porosity. Our model gives a different weight to the different porosities; the thermal conductivity varies linearly with the intraparticle porosity and varies critically with the interparticle porosity. The thermal conductivity can therefore be very variable with this pair even if the total porosity is constant. It can be seen that, for a total porosity of 0.7, the conductivity can vary from about 1 W(mK)$^{-1}$ to about 0.06 W(mK)$^{-1}$, depending if p_{inter} is equal to 0.25 or 0.5. This representation illustrates the importance of these two microstructural parameters (p_{inter} and p_{intra}) on the conductivity in a particle bed. The interval [0.25,0.5] is chosen because it frames the values of the measurements we have studied. Furthermore, it corresponds to the interparticle porosity values of systems composed of mono-dispersed dense spheres with arrangements ranging from simple cubic ($p_e = 0.48$) to face-centered cubic ($p_e = 0.26$).

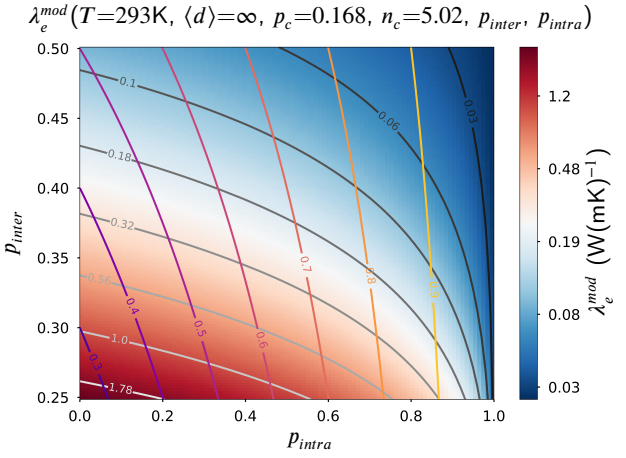

Figure 8: Thermal conductivity predicted by our model as a function of interparticle and intraparticle porosity. $\lambda_{air} = 0.025$ W(mK)$^{-1}$, $\lambda_{sc} = 36.6$ W(mK)$^{-1}$, and $p_c = 0.168$, $n_c = 5.02$. The grey lines are iso conductivity, the other lines (yellow, pink) are iso total porosity.

5. Conclusion

In our study, we measured thermal conductivities in different α-alumina powders at ambient pressure and in air, using an unsteady hot plane setup. We also took into account other values from the literature. These experimental data allowed us to verify the validity of the effective thermal conductivity model we developed for powder beds. In this model, we interpret the variations of the thermal diffusivity of a powder bed as a function of porosity as a second order transition. This model is a multi-scale description of the thermal conductivity in this type of material. Starting from the quantum scale, a purely theoretical value of the thermal conductivity of the pure compound (α-alumina) is given. Then, the microstructure is taken in the following set of parameters:

- Grain size, $\langle d \rangle$
- Intraparticle porosity, p_{intra}
- Interparticle porosity, p_{inter}
- Critical porosity, p_c

This allows us to be more consistent with the physical reality of porous systems with unconnected solid phases. This model allows us to predict the thermal conductivity of a powder bed to the nearest $\pm$0.1 W(mK)$^{-1}$ assuming that the interparticle porosity varies between 0.33 and 0.42. It forecasts the degradation of the bed conductivity to within 0.3%, compared to the theoretical conductivity of the pure crystal (ratio between the measurements and the model for measurements found in literature (part 4). Assuming a dense particle bed ($p_{inter} = p_e$), we compared our model to existing classical models, which do not take into account the distinction between intraparticle and interparticle porosity. Whether they are theoretical models or experimental correlations, they are not consistent over the whole porosity range ([0, 1]), unlike ours. The conductivity of ultra-porous powders is therefore better described by our model. The values chosen for the critical porosity p_c and for the critical exponent n_c can be discussed, since they were fixed without exact knowledge of the microstructural arrangement of all the beds studied. However, the values were not chosen randomly and seem to be in agreement with almost all measurements. The critical porosity is set by analogy with those obtained in previous studies on sintered material based on spherical particles. It corresponds to the site percolation threshold of centered cubic arrangement i.e with an effective coordination number equal to 14 (8 first and 6 second neighbors). Overall, the critical porosity can be considered as an adjustable parameter of the proposed model provided that sufficient information on the microstructural parameters of the solid system is available. We therefore agreed that most of the beds studied have a critical porosity of 0.168 and that the critical exponent in alumina is 5 (which can be compared to second order phase transitions). The original approach used by our model to describe heat transfer in porous media with unconnected solid phase seems to be validated. We plan to apply this method in a broader framework, for measurements carried out under more varied conditions (different gases and pressures).

Acknowledgements

The authors are grateful for the financial support provided by the French Alternative Energies and Atomic Energy Commission (CEA), Électricité de France (EDF) and FRAMATOME. The project leading to this publication has received funding from the Excellence Initiative of Aix-Marseille University - A*Midex, a French Investissements

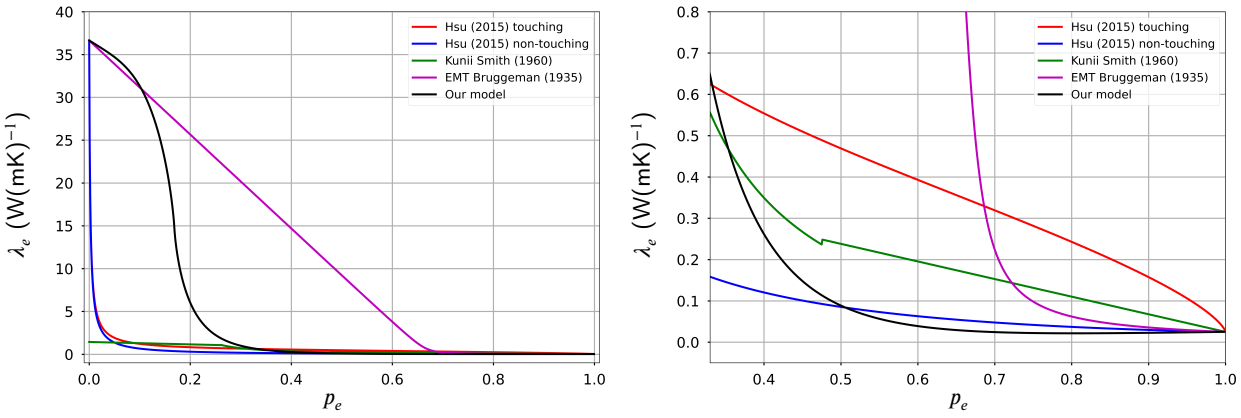

(a) (b)

Figure 9: Thermal conductivity as a function of porosity for different models with the same entry parameters. $\lambda_{air} = 0.025$ W(mK)$^{-1}$, $\lambda_{sc} = 36.6$ W(mK)$^{-1}$, $\lambda_p = \lambda_{sc}$ and $N(p_e, p_c = 0.168, n_c = 5.02)$ for our model. 9a corresponds to the model calculated over the entire porosity range, 9b is a zoom for $p_e \in [0.33, 1]$

dAvenir program AMX-19-IET-013. A.E.G and J. L acknowledge the support from the Natural Sciences and Engineering Research Council of Canada (NSERC), Rio Tinto Aluminium, Alcoa, Hydro Aluminium, Elysis and Constellium. The authors would like to thank E. Belisle for her valuable help in the proofreading of the manuscript and M. Soulon for his help in the sample granulometry characterization and Alteo-alumina compagny for providing us with various samples.

CRediT authorship contribution statement

Jordan Letessier: Conceptualization, Methodology, Validation, Software, Formal analysis, Investigation, Data curation, Writing original draft, Visualization. Aimen E Gheribi: Conceptualization, Methodology, Validation, Software, Formal analysis, Investigation, Data curation, Writing original draft, Visualization, Supervision. Jean-Mathieu Vanson: Investigation, Data curation, Resources, Writing review and editing. Christelle Duguay: Formal analysis, Data curation, Writing review and editing, Resources. Fabrice Rigollet: Investigation, Formal analysis, Data curation, Visualization, Writing review and editing, Resources. Nathalie Ehret: Formal analysis, Data curation, Visualization. Jerome Vicente: Formal analysis, Data curation, Visualization, Resources. Jean-Laurent Gardarein: Conceptualization, Methodology, Formal analysis, Investigation, Data curation, Resources, Writing original draft, Project administration, Supervision.

Declaration of Competing Interest

The authors declare that they have no known competing financial interests or personal relationships that could have appeared to influence the work reported in this paper.

References

Aster, R.C., Borchers, B., Thurber, C.H., 2018. Parameter estimation and inverse problems. Elsevier.

Boegli, J.S., Deissler, R.G., 1955. Measured effective thermal conductivity of uranium oxide powder in various gases and gas mixtures .

Bricout, J., Gelin, J.C., Ablitzer, C., Matheron, P., Brothier, M., 2013. Influence of powder characteristics on the behaviour of PIM feedstock. Chemical Engineering Research and Design 91, 2484–2490. Publisher: Elsevier.

Bruggeman, D.a.G., 1935. Berechnung verschiedener physikalischer Konstanten von heterogenen Substanzen. I. Dielektrizitätskonstanten und Leitfähigkeiten der Mischkörper aus isotropen Substanzen. Annalen der Physik 416, 636–664. URL: https://onlinelibrary.wiley.com/doi/abs/10.1002/andp.19354160705, doi:10.1002/andp.19354160705. _eprint: https://onlinelibrary.wiley.com/doi/pdf/10.1002/andp.19354160705.

De Hoog, F.R., Knight, J.H., Stokes, A.N., 1982. An improved method for numerical inversion of Laplace transforms. SIAM Journal on Scientific and Statistical Computing 3, 357–366. doi:https://doi.org/10.1137/0903022. publisher: SIAM.

Deprez, N., McLachlan, D.S., Sigalas, I., 1989. The measurement and comparative analysis of the electrical and thermal conductivities and permeability of sintered nickel. Physica A: Statistical Mechanics and its Applications 157, 181–184. URL: https://www.sciencedirect.com/science/article/pii/0378437189902975, doi:10.1016/0378-4371(89)90297-5.

Dullien, F.A., 2012. Porous media: fluid transport and pore structure. Academic press.

Francl, J., Kingery, W.D., 1954. Thermal conductivity: IX, experimental investigation of effect of porosity on thermal conductivity. Journal of the American ceramic Society 37, 99–107. doi:https://doi.org/10.1111/j.1551-2916.1954.tb20108.x. publisher: Wiley Online Library.

Ghanbarian, B., Daigle, H., 2016. Thermal conductivity in porous media: Percolation-based effective-medium approximation. Water Resources Research 52, 295–314. URL: https://onlinelibrary.wiley.com/doi/abs/10.1002/2015WR017236, doi:10.1002/2015WR017236. _eprint: https://onlinelibrary.wiley.com/doi/pdf/10.1002/2015WR017236.

Gheribi, A.E., Chartrand, P., 2012. Application of the CALPHAD method to predict the thermal conductivity in dielectric and semiconductor crystals. Calphad 39, 70–79. URL: https://www.sciencedirect.com/science/article/pii/S0364591612000508, doi:10.1016/j.calphad.2012.06.002.

Gheribi, A.E., Chartrand, P., 2015. Effect of Grain Boundaries on the Lattice Thermal Transport Properties of Insulating Materials: A Predictive Model. Journal of the American Ceramic Society 98,

888–897. URL: https://ceramics.onlinelibrary.wiley.com/doi/abs/10.1111/jace.13338, doi:https://doi.org/10.1111/jace.13338. _eprint: https://ceramics.onlinelibrary.wiley.com/doi/pdf/10.1111/jace.13338.

Gheribi, A.E., Gardarein, J.L., Autissier, E., Rigollet, F., Richou, M., Chartrand, P., 2015. Experimental study of the thermal conductivity of sintered tungsten: Evidence of a critical behaviour with porosity. Applied Physics Letters 107, 094102. doi:https://doi.org/10.1063/1.4929717. publisher: AIP Publishing LLC.

Gheribi, A.E., Gardarein, J.L., Rigollet, F., Chartrand, P., 2014. Evidence of second order transition induced by the porosity in the thermal conductivity of sintered metals. APL Materials 2, 076105. doi:https://doi.org/10.1063/1.4886221. publisher: American Institute of Physics.

Giraud, M., Gatumel, C., Vaudez, S., Bernard-Granger, G., Nos, J., Gervais, T., Berthiaux, H., 2020. Investigation of a granular Bond number based rheological model for polydispersed particulate systems. Chemical Engineering Science 228, 115971. Publisher: Elsevier.

Hadley, G.R., 1986. Thermal conductivity of packed metal powders. International Journal of Heat and Mass Transfer 29, 909–920. URL: https://www.sciencedirect.com/science/article/pii/0017931086901869, doi:10.1016/0017-9310(86)90186-9.

Hashin, Z., Shtrikman, S., 1962. A Variational Approach to the Theory of the Effective Magnetic Permeability of Multiphase Materials. Journal of Applied Physics 33, 3125–3131. URL: http://aip.scitation.org/doi/10.1063/1.1728579, doi:10.1063/1.1728579.

Hsu, C.T., Cheng, P., Wong, K.W., 1995. A Lumped-Parameter Model for Stagnant Thermal Conductivity of Spatially Periodic Porous Media. Journal of Heat Transfer 117, 264–269. URL: https://doi.org/10.1115/1.2822515, doi:10.1115/1.2822515.

Hu, X.J., Prasher, R., Lofgreen, K., 2007. Ultralow thermal conductivity of nanoparticle packed bed. Applied Physics Letters 91, 203113. URL: http://aip.scitation.org/doi/10.1063/1.2814959, doi:10.1063/1.2814959.

Huang, L., El-Genk, M.S., 2001. Thermal conductivity measurements of alumina powders and molded Min-K in vacuum. Energy Conversion and Management , 14.

Inden, G., 1976. Project Meeting Calphad V. Ch. 111 4, 1–13.

Jerauld, G.R., Scriven, L.E., Davis, H.T., 1984. Percolation and conduction on the 3D Voronoi and regular networks: a second case study in topological disorder. Journal of Physics C: Solid State Physics 17, 3429–3439. URL: https://doi.org/10.1088/0022-3719/17/19/017, doi:10.1088/0022-3719/17/19/017. publisher: IOP Publishing.

Julian, C.L., 1965. Theory of heat conduction in rare-gas crystals. Physical Review 137, A128. doi:https://doi.org/10.1103/PhysRev.137.A128. publisher: APS.

Kunii, D., Smith, J.M., 1960. Heat transfer characteristics of porous rocks. AIChE Journal 6, 71–78. URL: https://aiche.onlinelibrary.wiley.com/doi/abs/10.1002/aic.690060115, doi:10.1002/aic.690060115. _eprint: https://aiche.onlinelibrary.wiley.com/doi/pdf/10.1002/aic.690060115.

Lager, D., KNOLL, C., MULLER, D., HOHENAUER, W., WEINBERGER, P., WERNER, A., 2019. Thermal conductivity measurements of calcium oxalate monohydrate as thermochemical heat storage material. Thermal Conductivity 33/Thermal Expansion 21 .

Lahoori, M., Jannot, Y., Rosin-Paumier, S., Boukelia, A., Masrouri, F., 2020. Measurement of the thermal properties of unsaturated compacted soil by the transfer function estimation method. Applied Thermal Engineering 167, 114795. Publisher: Elsevier.

Laubitz, M.J., 1959. Thermal conductivity of powders. Canadian Journal of Physics 37, 798–808. doi:https://doi.org/10.1139/p59-086. publisher: NRC Research Press Ottawa, Canada.

Lemmon, E.W., Jacobsen, R.T., 2004. Viscosity and Thermal Conductivity Equations for Nitrogen, Oxygen, Argon, and Air. International Journal of Thermophysics 25, 21–69. URL: http://link.springer.com/10.1023/B:IJOT.0000022327.04529.f3, doi:10.1023/B:IJOT.0000022327.04529.f3.

Li, S., Wang, C.A., Zhou, J., 2013. Effect of starch addition on microstructure and properties of highly porous alumina ceramics. Ceramics International 39, 8833–8839. URL: https://www.sciencedirect.com/science/article/pii/S0272884213004732, doi:10.1016/j.ceramint.2013.04.072.

Luikov, A.V., Shashkov, A.G., Vasiliev, L.L., Fraiman, Y.E., 1968. Thermal conductivity of porous systems. International Journal of Heat and Mass Transfer 11, 117–140. URL: https://www.sciencedirect.com/science/article/pii/0017931068901440, doi:10.1016/0017-9310(68)90144-0.

Maillet, D., André, S., Batsale, J.C., Degiovanni, A., Moyne, C., 2000. Solving the heat equation through integral transforms. Edition Wiley .

Maillet, D., Jannot, Y., Degiovanni, A., 2013. Analysis of the estimation error in a parsimonious temperature-temperature characterization technique. International Journal of Heat and Mass Transfer 62, 230–241. doi:https://doi.org/10.1016/j.ijheatmasstransfer.2013.02.055. publisher: Elsevier.

Masamune, S., Smith, J.M., 1963. Thermal Conductivity of Beds of Spherical Particles. Industrial & Engineering Chemistry Fundamentals 2, 136–143. URL: https://pubs.acs.org/doi/abs/10.1021/i160006a009, doi:10.1021/i160006a009.

McLachlan, D.S., 1987. An equation for the conductivity of binary mixtures with anisotropic grain structures. Journal of Physics C: Solid State Physics 20, 865–877. URL: https://iopscience.iop.org/article/10.1088/0022-3719/20/7/004, doi:10.1088/0022-3719/20/7/004.

Oberlænder, B.C., Wiesenack, W., 2014. Overview of Halden reactor LOCA experiments (with emphasis on fuel fragmentation) and plans. Institutt for energiteknikk.

Polamuri, D., Thamida, S.K., 2015. Experimental determination of effective thermal conductivity of granular material by using a cylindrical heat exchanger. International Journal of Heat and Mass Transfer 81, 767–773. URL: https://www.sciencedirect.com/science/article/pii/S0017931014009661, doi:10.1016/j.ijheatmasstransfer.2014.10.070.

Predeep, P., Saxena, N.S., 1997. Effective thermal conductivity and thermal diffusivity of some rare earth oxides. Physica Scripta 55, 634. Publisher: IOP Publishing.

Pujula, M., Sánchez-Rodríguez, D., Lopez-Olmedo, J.P., Farjas, J., Roura, P., 2016. Measuring thermal conductivity of powders with differential scanning calorimetry. Journal of Thermal Analysis and Calorimetry 125, 571–577. Publisher: Springer.

Rigollet, F., Le Niliot, C., 2011. Front Face Thermal Characterization of Materials by a Photothermal Pulse Technique, in: Thermal Measurements and Inverse Techniques. CRC Press, pp. 669–688.

Sciamanna, V., Nait-Ali, B., Gonon, M., 2015. Mechanical properties and thermal conductivity of porous alumina ceramics obtained from particle stabilized foams. Ceramics International 41, 2599–2606. doi:https://doi.org/10.1016/j.ceramint.2014.10.011. publisher: Elsevier.

Shapiro, M., Dudko, V., Royzen, V., Krichevets, Y., Lekhtmakher, S., Grozubinsky, V., Shapira, M., Brill, M., 2004. Characterization of powder beds by thermal conductivity: effect of gas pressure on the thermal resistance of particle contact points. Particle & Particle Systems Characterization: Measurement and Description of Particle Properties and Behavior in Powders and Other Disperse Systems 21, 268–275. Publisher: Wiley Online Library.

Shimizu, T., Matsuura, K., Furue, H., Matsuzak, K., 2013. Thermal conductivity of high porosity alumina refractory bricks made by a slurry gelation and foaming method. Journal of the European ceramic Society 33, 3429–3435. doi:https://doi.org/10.1016/j.jeurceramsoc.2013.07.001. publisher: Elsevier.

Sosoi, G., Abid, C., Barbuta, M., Burlacu, A., Balan, M.C., Branoaea, M., Vizitiu, R.S., Rigollet, F., 2022. Experimental Investigation on Mechanical and Thermal Properties of Concrete Using Waste Materials as an Aggregate Substitution. Materials 15, 1728. Publisher: MDPI.

Stepanenko, O., Tartari, A., Amamra, M., Nguyen, T.H.N., Piat, M., Favero, I., Ducci, S., Khodan, A., Boinovich, L.B., Emelyanenko, A.M., 2015. Ultra-porous alumina for microwave planar antennas. Advanced Device Materials 1, 93–99. Publisher: Taylor & Francis.

Sun, J., Hu, Z., Zhuo, J., Wang, X., Sun, C., 2014. Thermal properties of highly porous fibrous ceramics .

Van Der Marck, S.C., 1998. Calculation of Percolation Thresholds in High Dimensions for FCC, BCC and Diamond Lattices. International Journal of Modern Physics C 09, 529–540. URL: https://www.worldscientific.com/doi/abs/10.1142/S0129183198000431, doi:10.

1142/S0129183198000431. publisher: World Scientific Publishing Co.

Van Norman, S.A., Tringe, J.W., Sain, J.D., Yang, R., Falconer, J.L., Weimer, A.W., 2015. Using atomic layer deposited tungsten to increase thermal conductivity of a packed bed. Applied Physics Letters 106, 153102. URL: http://aip.scitation.org/doi/10.1063/1.4917309, doi:10.1063/1.4917309.

Yagi, S., Kunii, D., 1957. Studies on effective thermal conductivities in packed beds. AIChE Journal 3, 373–381. URL: https://aiche.onlinelibrary.wiley.com/doi/abs/10.1002/aic.690030317, doi:10.1002/aic.690030317. _eprint: https://aiche.onlinelibrary.wiley.com/doi/pdf/10.1002/aic.690030317.

Zehner, P., Schlünder, E.U., 1970. Wärmeleitfähigkeit von Schüttungen bei mäßigen Temperaturen. Chemie Ingenieur Technik 42, 933–941. URL: https://onlinelibrary.wiley.com/doi/abs/10.1002/cite.330421408, doi:10.1002/cite.330421408. _eprint: https://onlinelibrary.wiley.com/doi/pdf/10.1002/cite.330421408.

A. Appendix

Table 2
Models

Reference	Expression of λ_e^{mod}
Bruggeman (1935)	$(1-p_e)\dfrac{\lambda_{sc}-\lambda_e^{mod}}{\lambda_{sc}+2\lambda_e^{mod}}+p_e\dfrac{\lambda_{air}-\lambda_e^{mod}}{\lambda_{air}+2\lambda_e^{mod}}=0$
Kunii and Smith (1960)	$\lambda_e^{mod}/\lambda_{air}=p_e+\beta(1-p_e)/(\psi_t+\gamma/\kappa),\ \kappa=\lambda sc/\lambda air$
	$\begin{cases}\beta=0.895,\ n_2=4\sqrt{3},\ \psi_t=\psi_2 & \text{for } p_e<0.26\\ \beta=1,\ n_1=1.5,\ \psi_t=\psi_1 & \text{for } p_e\geq 0.476\\ \beta=0.486(p_e-0.26)+0.895,\ \psi_t=\psi_2+(\psi_1-\psi_2)(p_e-0.26)/0.216 & \text{for } 0.26\leq p_e\leq 0.476\end{cases}$
	$\psi_{1or2}=\dfrac{0.5*((\kappa-1)/\kappa)^2\sin^2\theta_0}{\ln(\kappa-(\kappa-1)\cos\theta_0)-(\kappa-1)/\kappa\ (1-\cos\theta_0)}-\dfrac{2}{3\kappa},\ \sin^2\theta_0=1/n_{1or2}$
Hsu et al. (1995) (touching cubes)	$\lambda_e^{mod}/\lambda_{air}=1-\gamma_a^2-2\gamma_c\gamma_a+2\gamma_c\gamma_a^2+(\gamma_c\gamma_a)^2\kappa+\dfrac{\gamma_c^2-(\gamma_c\gamma_a)^2}{1-\gamma_a+\gamma_a/\kappa}+\dfrac{2(\gamma_c\gamma_a-\gamma_c\gamma_a^2)}{1-\gamma_c\gamma_a+\gamma_c\gamma_a/\kappa}$
	With $1-p_e=(1-3\gamma_c^2)\gamma_a^3+3(\gamma_c\gamma_a)^2$ and $\gamma_c=0.13$
Hsu et al. (1995) (non-touching cubes)	$\lambda_e^{mod}/\lambda_{air}=(1-(1-p_e)^{2/3})+\dfrac{(1-p_e)^{2/3}}{1+(1/\kappa-1)(1-p_e)^{1/3}}$